Seasonal Variations of Upper Ocean Transport from the Pacific to the Indian Ocean via Indonesian Straits*

JAMES T. POTEMRA

International Pacific Research Center, University of Hawaii at Manoa, Honolulu, Hawaii

(Manuscript received 13 July 1998, in final form 6 January 1999)

ABSTRACT

Seasonal variations of upper-ocean mass transport between the Pacific and Indian Oceans via the Indonesian Throughflow (ITF) are examined using numerical experiments with a 1½-layer, reduced-gravity model forced with specific climatological winds. The model ITF transport, computed as a sum of through-strait transport, has an annual range of more than 8 Sv (an annual harmonic of amplitude 4.2 Sv and a smaller, semiannual harmonic amplitude of 0.5 Sv (Sv $\equiv 10^6$ m^3 s^{-1}), with peak transport from mid-April through July and minimum transport in November and December. Limited long-term observations make it difficult to validate these results, but they are consistent with current theory. Experiments with time-varying winds in specific regions show that most of the annual throughflow signal is due to equatorial winds (from 10°S to 10°N); ITF transport anomalies generated by off-equatorial winds account for less than 1 Sv and are mostly out of phase with the baseline throughflow signal. For the particular wind data used in this study, effects of remote wind forcing in the equatorial Indian Ocean are countered by local winds in the Indonesian seas, and the annual cycle of through-strait transport derived from the model forced only by equatorial Pacific winds is nearly equivalent to that of the baseline run. In this model, the specified wind stress causes annual Rossby waves to be formed in the eastern Pacific by Ekman pumping. These Rossby waves propagate to the western boundary of the Pacific, then form coastal Kelvin waves that propagate through the Indonesian seas. In northern spring, a downwelling wave brings elevated sea level to the Pacific side of the Indonesian seas, and the ITF is maximum. In northern fall an upwelling wave reduces the sea level on the Pacific side, and ITF transport is minimum. In the Indian Ocean, monsoon winds produce equatorial Kelvin waves that propagate eastward and form coastal waves along the southern coasts of Sumatra and Java. A downwelling (upwelling) wave increases (decreases) sea level on the Indian Ocean side of Indonesia in northern spring (winter), thus acting in opposition to the baseline ITF variability. The effect of local Ekman pumping is in the opposite sense. In northern winter, when remote Indian Ocean winds create an upwelling coastal wave, the local wind stress provides downward Ekman pumping. In northern spring, locally forced, upward Ekman suction counters the remotely forced, downwelling Kelvin wave.

1. Motivation

Recently, the Indonesian Throughflow (ITF) has received attention because of its potential role in removing heat from the western Pacific (e.g., Qu et al. 1994). In the coupled model results of Schneider and Barnett (1997), 0.9 PW of heat was exported from the western Pacific via the model's ITF. Computations from the Parallel Ocean Climate Model (POCM) of Semtner and Chervin (1988) show an annual mean of 1 PW. For comparison, this is equivalent to a 25 W m^{-2} heat flux over the surface area of the Indonesian seas (taken to be approximately 4×10^{13} m^2). More important for climate is the variability of this heat flux. The POCM results show significant interannual variability (about 1 PW) as well as a strong seasonal signal, sometimes as large as 2 PW. This heat flux represents an important component of the ocean heat budget in the western Pacific.

Another important component of the regional heat budget is the surface heat flux. This is primarily tied to the SSTs in the region and provides the link to the atmosphere. For example, SSTs in the Indonesian seas could be a key factor for driving the Asian–Australian (A–A) monsoons. Further, Nicholls (1984) showed that SST anomalies in the Indonesian region are related to ENSO phenomena.

The exact relationship between the ITF, SSTs, and heat fluxes in the western Pacific/Indonesian seas region is still under investigation. Before this complex, inherently coupled problem can be solved, the dynamics that control the variability of the ITF must be understood and properly simulated. Several observational efforts have focused on this region, but available long-term data

* SOEST Contribution Number 4738.

Corresponding author address: Dr. James T. Potemra, University of Hawaii at Manoa, SOEST/IPRC, 1000 Pope Road, Honolulu, HI 96822.
E-mail: jimp@hawaii.edu

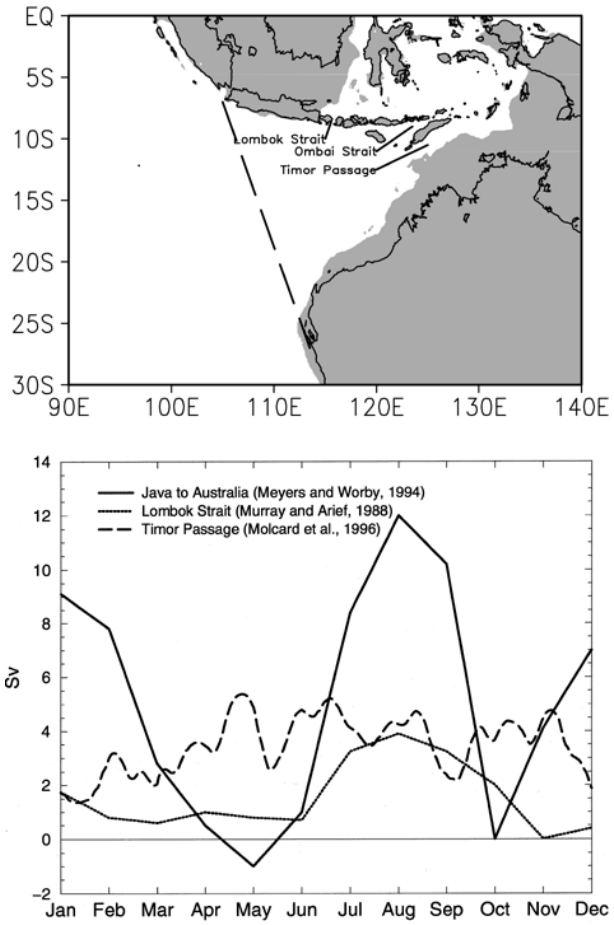

FIG. 1. The upper panel shows where observations of throughflow variability have been made. Depths less than 200 m have been shaded. The dashed line shows the XBT track of Meyers et al. (1995). The lower panel shows the throughflow transports. The solid line is monthly mean throughflow transport (in Sv) computed from a six-year XBT repeat section depth (reproduced from Meyers et al. 1995). The dotted line is transport based on measurements in the Lombok Strait during 1985 by Murray and Arief (1988). The dashed line represents measurements made by current meters (0 to 500 m) in the Timor Passage during 1992 (Molcard et al. 1996). Positive values indicate flow from the Pacific to the Indian Ocean.

are still very limited. Many advances in understanding throughflow dynamics have been made using theoretical considerations, and numerical model advances have contributed. Despite all the recent work, the long-term mean ITF transport, the annual and interannual variability of this transport, and what effect this variability has on climate are still not clear.

The focus of this particular study is ITF variability on the timescale of months, that is, the seasonal cycle. For the purpose of this study, the problem is investigated from a purely oceanic context. Only hydrodynamic forcing is considered in an attempt to discern the dynamics that control the ITF on the annual timescale (this assumption is addressed in section 3). In addition, only upper-ocean variability is studied, for it assumed that this will have the greatest impact on SSTs in the region. There is certainly a difference between the barotropic and baroclinic response of the ITF (e.g., Schneider and Barnett 1997; Schiller et al. 1998). This is discussed further in section 2c using results from a large-scale OGCM. Finally, for the purposes of this study, throughflow transport is computed as a sum of transport through three main straits in the Malay Archipelago. A long-term estimate of throughflow transport based on observations has been made (Meyers et al. 1995). This estimate, however, is along a track from Java to Australia to the west of the Indonesian straits (these observations are discussed in section 2a). There are several processes that could control storage of upper-ocean waters between these two locations (e.g., the thermally driven Leeuwin Current, the South Java Current, large-scale Indian Ocean currents, etc.). This is the focus of a future study.

Unlike previous modeling studies, this effort employs a relatively simple model run under numerous configurations to gain a better understanding of the dynamics controling seasonal fluctuations in the ITF and to determine what processes are important for correctly simulating the ITF. The next section provides a background, citing previous observational, theoretical, and numerical efforts. This is followed by a description of the model used in this study and an outline of the experiments run. Some results and hypotheses are then presented.

2. Background

Despite the recent attention to circulation in the Indonesian region, there are still relatively few measurements or estimates of transport there. A complete discussion is given in Lukas et al. (1996) and in Godfrey (1996). Here, the discussion is limited to the observational, theoretical, and model studies where the variation of the ITF on annual timescales is either directly presented or can be inferred.

a. Observations

There are few observations of the upper-ocean transport between the Pacific and Indian Oceans of long enough duration to address the issue of annual variability. An exception are the estimates of Meyers et al. (1995) based on six years (1983 through 1989) of expendable bathythermograph (XBT) sections from Australia (Shark Bay) to the Sunda Strait (between Sumatra and Java). These data were used with climatological temperature and salinity profiles to calculate geostrophic velocity relative to 400 m. The long-term mean was estimated to be 5 Sv (Sv $\equiv 10^6$ m^3 s^{-1}), with both a strong semiannual and annual component. The annual maximum (12 Sv) was found to be in August/September and the minimum in May was -2 Sv (flow toward the Pacific). Figure 1 shows the six-year mean annual climatology. The interannual variability of this signal is

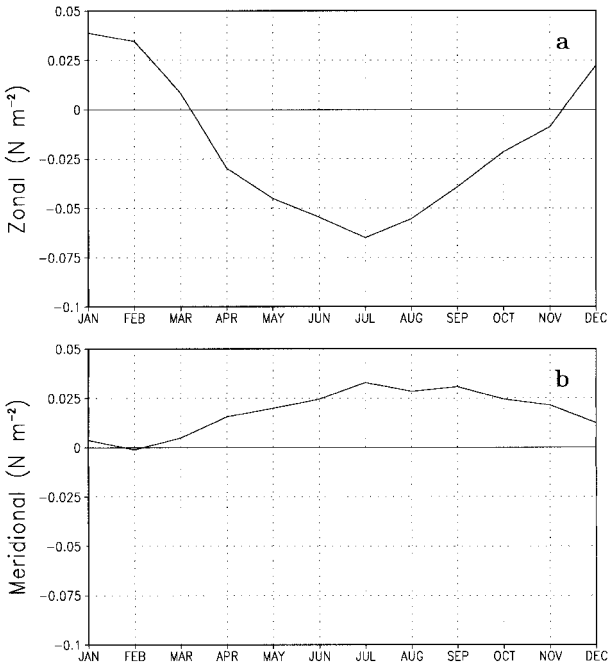

FIG. 2. Area mean wind stress was computed from the Hellerman and Rosenstein (1983) dataset in the throughflow region (105°–130°E, 15°–5°S). The upper panel (a) shows the zonal wind stress (in N m^{-2}), and the lower panel shows the meridional component. Positive values indicate wind stress toward the east and north, respectively.

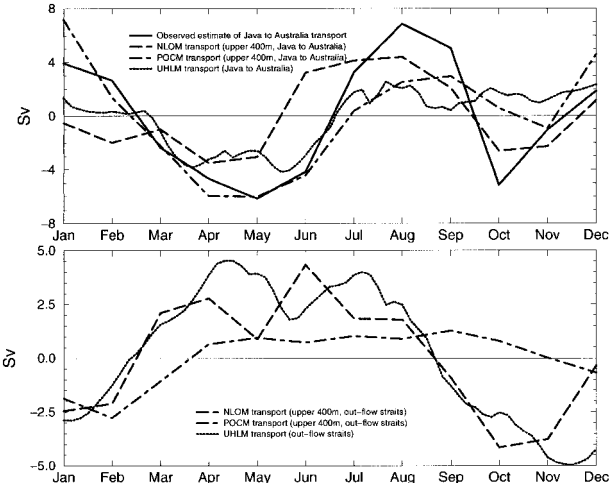

FIG. 3. Seasonal transport variations are shown from three models and the observations of Meyers et al. (1995). In each case, a climatology was made from depth-integrated transport over the top 400 m from observations (solid line), NLOM (dashed line), the POCM (dash–dotted line), and the UHLM (dotted line). In each case the long-term mean has been subtracted. The top panel is transport computed along the Java to Australia track, and the bottom panel is transport computed as a sum of the three outflow straits (see Fig. 1 for locations).

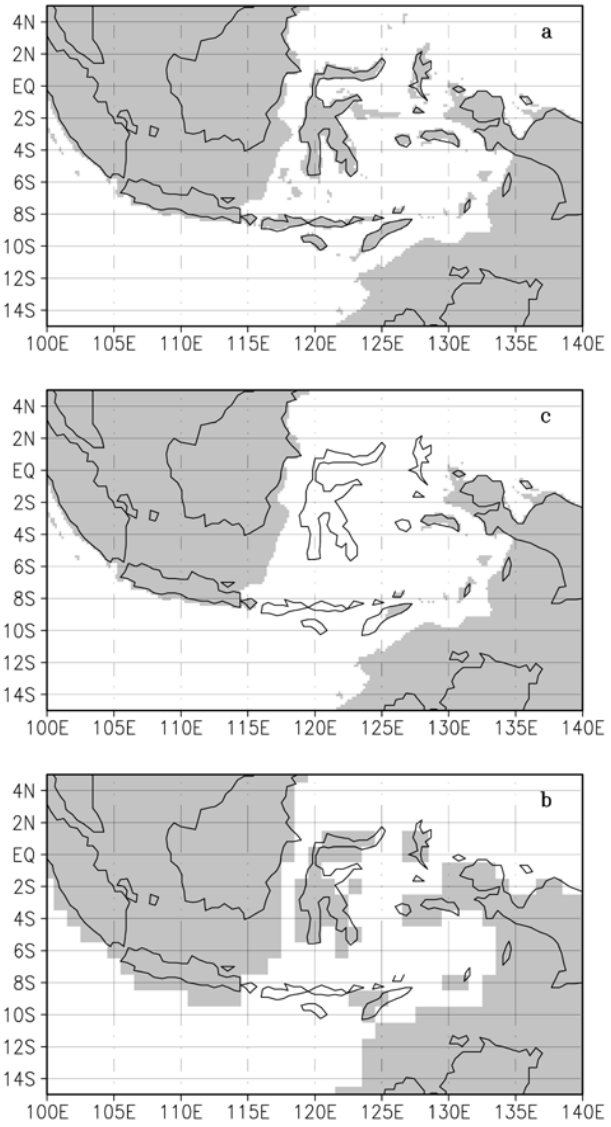

FIG. 4. The three model grids used are shown for the ITF region. Model land points are shaded, and a geographic map is drawn for reference. The upper panel (a) is for the ⅙° by ⅙° experiments, the center panel (b) shows the grid for the experiment with an artificially wide ITF region (also ⅙° by ⅙°), and the lower panel (c) shows the grid for the coarse-resolution run (1° by 1°).

discussed in Meyers (1996) with data from 1983 through 1994.

Transport variability based on these observations (which are along a section from Java to Australia) may or may not be indicative of transport variability in the various Indonesian straits (through-strait transport). The XBT line is more than 10° west of the Indonesian straits, and the issue of storage of surface waters is important. Both ends of the section are subject to boundary currents (the South Java Current at the north end and the Leeuwin Current at the south end). Additionally, the Indian Ocean subtropical gyre may intrude across this section from the east.

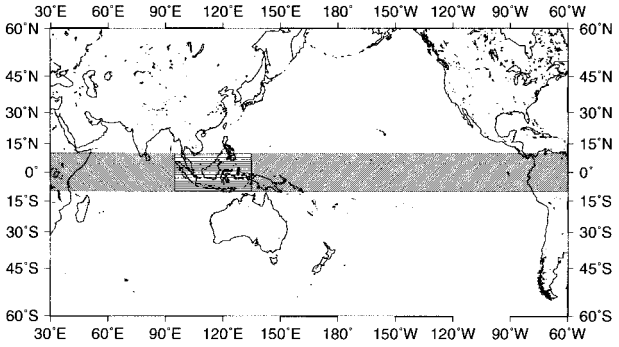

FIG. 5. Time-varying winds were applied to the UHLM over the three different shaded regions in several different model runs. In each case, December mean winds were applied everywhere else. Additional runs were made with time-varying winds over the entire shaded region and time-varying winds everywhere not shaded. (Note: the model domain extends farther south than shown above.)

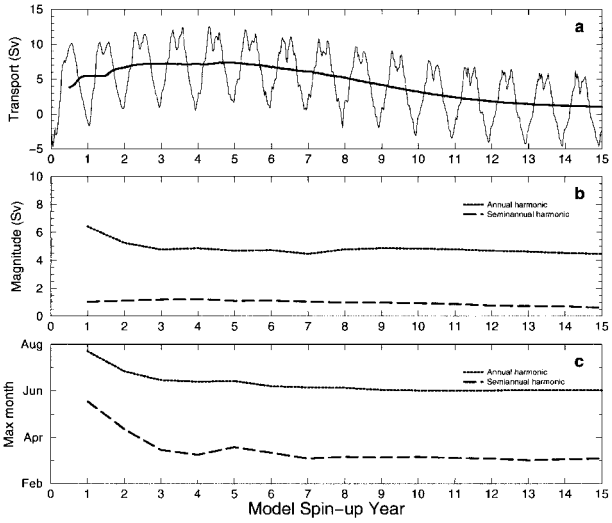

FIG. 6. The top panel (a) shows the Indonesian Throughflow transport (thin line) and 12-month running mean (heavy line) computed from the nonlinear model integration from rest. Negative values indicate flow from the Pacific to the Indian Ocean. The center panel (b) shows the magnitude of the annual and semiannual harmonics of the transport in the top panel, and the lower panel (c) gives the phase (plotted as the month when the harmonics are maximum). The annual harmonic is given by the dotted line, and the semiannual harmonic is given by the dashed line.

A yearlong current meter record (Murray and Arief 1988) of upper-ocean flow (top 800 m) in the Lombok Strait shows that this particular strait had a 1985 mean of 2 Sv and the signal was mainly annual. The peak transport was observed in August, similar to the Meyers et al. (1995) results. The results are also displayed in Fig. 1.

Observations in the Timor Passage were made with current meter moorings from April 1992 through April 1993 (Molcard et al. 1996). The upper-ocean transport variations (transport in the top 500 m is shown in Fig. 1) show strong intraseasonal variability [see Qiu et al. (1998) for a discussion of this variability], with a less apparent annual cycle. Transport is generally high in April through November (about 4 Sv) and low in December though March (about 2 Sv). Interestingly, transport in a subsurface layer [500–1250 m (not shown here)] shows a strong semiannual signal, slightly larger in magnitude to the surface fluctuations (from almost 5 Sv in May and June to -0.5 Sv in August). Transport variability below 1250 m is less than 1 Sv.

On the southern side of Indonesia, long-term drifter measurements of Quadfasel and Cresswell (1992) show a seasonally reversing South Java Current (SJC). This current flows along the southern coast of Sumatra/Java, toward the east in boreal winter (October through May) and toward the west in boreal summer (May through September). The corresponding coastal sea level anomalies (from geostrophy) would therefore be positive (high) in northern winter and negative (low) in northern summer. The timing and direction of the SJC is due to a complex interaction between the monsoonal wind stress and baroclinic coastal waves. From November to February, the winds along the southern Sumatra/Java coast have a westerly component, while the rest of the year the winds are easterly.

b. Theoretical considerations

Theoretical studies have focused on a variety of factors. One early theory was put forth by Wyrtki (1961), who suggested that the ITF was driven mainly by the pressure difference between the Pacific and Indian Oceans. This pressure head is established by the easterly trades, which cause sea level to become higher on the Pacific Ocean side of the Malay Archipelago.

Figure 2 shows the area mean wind stress computed from the Hellerman and Rosenstein (1983) dataset. The

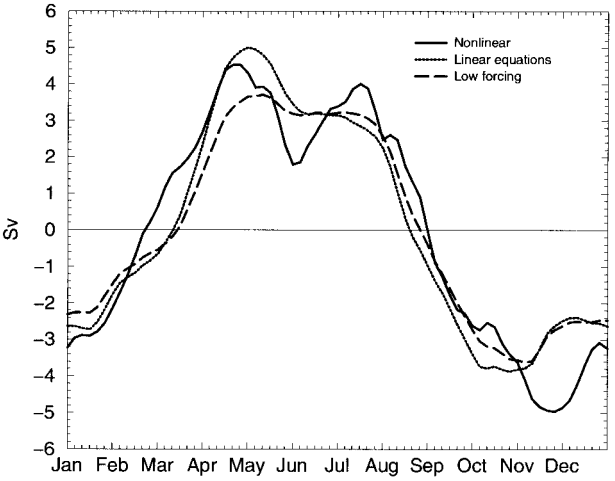

FIG. 7. ITF transport anomalies from the nonlinear run are given with the heavy line. Transport anomalies from the linear equations run are given by the dotted line, and anomalies from the low forcing run are given by the dashed line. The variations are plotted such that positive represents an increase in the flow from the Pacific to the Indian Ocean.

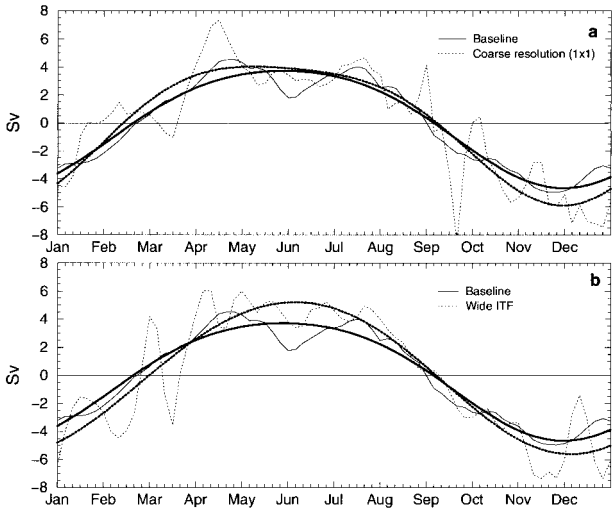

FIG. 8. Throughflow transports were computed from model experiments with two different grids. The upper panel (a) is from a coarse-resolution model run (1° by 1°). The lower panel is from the model run with a wide ITF region. In each panel, results from the baseline run are shown with the solid line, results from the specific experiment are shown with the dashed line, and the annual plus semiannual harmonics are shown with the thick lines.

mean was computed over a region including the Flores, Banda, and Timor Seas (from 15° to 5°S, 105° to 130°E). During November through March the winds are to the east, and surface flow is from the Java Sea (and Pacific) into the Banda Sea. Winds are not favorable to remove this water, and the resulting Ekman flow causes warm surface waters to accumulate in the Banda Sea and depress the thermocline there (Wyrtki 1987). Simultaneously, the large-scale pressure gradient from the Pacific to the Indian Ocean weakens [the intertropical convergence zone (ITCZ) is south of Java during this time]. Consequently, the upper-ocean ITF transport should be weak. During the northern summer monsoon, from May to September, the winds are more intense and to the northwest over the entire Indonesian region (see Fig. 2). At this time, the winds tend to remove surface water from the Banda Sea into the Indian Ocean. This should be when the upper-ocean ITF transport is strongest. It necessarily follows from this that the ITF (in the surface waters) should have mainly an annual period, coincident with the monsoonal change in winds.

Later theoretical studies have used the ''Island Rule'' (Godfrey 1989) to hypothesize that the long-term mean ITF is determined by the integral of wind stress along a closed path from the west coast of South America to the northern tip of New Guinea, south along the west coast of New Guinea and Australia, east from the southern tip of Tasmania to South America, then north along the coast. In the original work, Godfrey (1989) integrated the Sverdrup balance along this closed path. In following studies, the island rule was expanded to include bottom topography and friction (Wajsowicz 1993) and baroclinic effects (Wajsowicz 1995). Several other variations are described in (Pratt and Pedlosky 1998) and (Pedlosky et al. 1997). All principally rely on the path integral of wind stress to determine ITF transport, but none address seasonal variability of this signal.

The annual cycle of ITF transport was addressed by Clarke and Liu (1993) and Clarke and Liu (1994). In their theory, the interannual variations of the ITF were controlled by large-scale sea level on the Pacific Ocean side, similar to the conclusions of Wyrtki (1987), but annual variations were due to waves generated in the Indian Ocean. This leads to the possibility that waves on both sides of the Malay Archipelago could adjust sea level and thereby modulate ITF transport. It also presents the possibility that the ITF would have a semiannual component (due to semiannual signals in the Indian Ocean).

c. Previous modeling studies

Several numerical modeling studies have either focused directly on the Indonesian Through-flow or include this region in their domain. To highlight the uncertainty in throughflow variability, results from two OGCMs that have been used extensively to study global circulation problems are compared. The two models are the Parallel Ocean Climate Model (POCM) of Semtner and Chervin (1988) and the Navy Layered Ocean Model (NLOM) developed at the Naval Research Laboratory (Wallcraft 1991). The two models employ different numerical strategies, and previous validation of these models has been done on a global scale.

Two significant differences are in the model vertical coordinates and forcing. The POCM is a *z*-coordinate, level model (20 vertical levels). It has a horizontal resolution of 0.4° in the equatorial region. It was forced by twice daily, 10-m winds from the analyses of the European Centre for Medium-Range Weather Forecasts (ECMWF) [averaged to three days, converted to wind stress (Trenberth et al. 1990), then interpolated to the model time step]. Results for 1987 through 1995 are used in this comparison (nine years of monthly mean data).

The NLOM is a 5½-layer model. It is a reduced-gravity model, with the lowest layer at rest, so bottom topography is not incorporated. The model was forced with a hybrid wind product based on monthly anomalies from the 1000-mb ECMWF wind field added to the monthly mean, seasonal wind of Hellerman and Rosenstein (1983), so the interannual wind forcing is the same as the POCM, but the mean and annual variations are different. Ten years of data (monthly means from 1981 through 1990) are used to compute ITF transport.

Throughflow transport computed from the depth-integrated velocity fields of both models through the southern straits in Indonesia and along a transect similar to the Meyers et al. (1995) observations are shown in Fig. 3. The long-term mean has been removed in each case. In order to compare with the observations, only

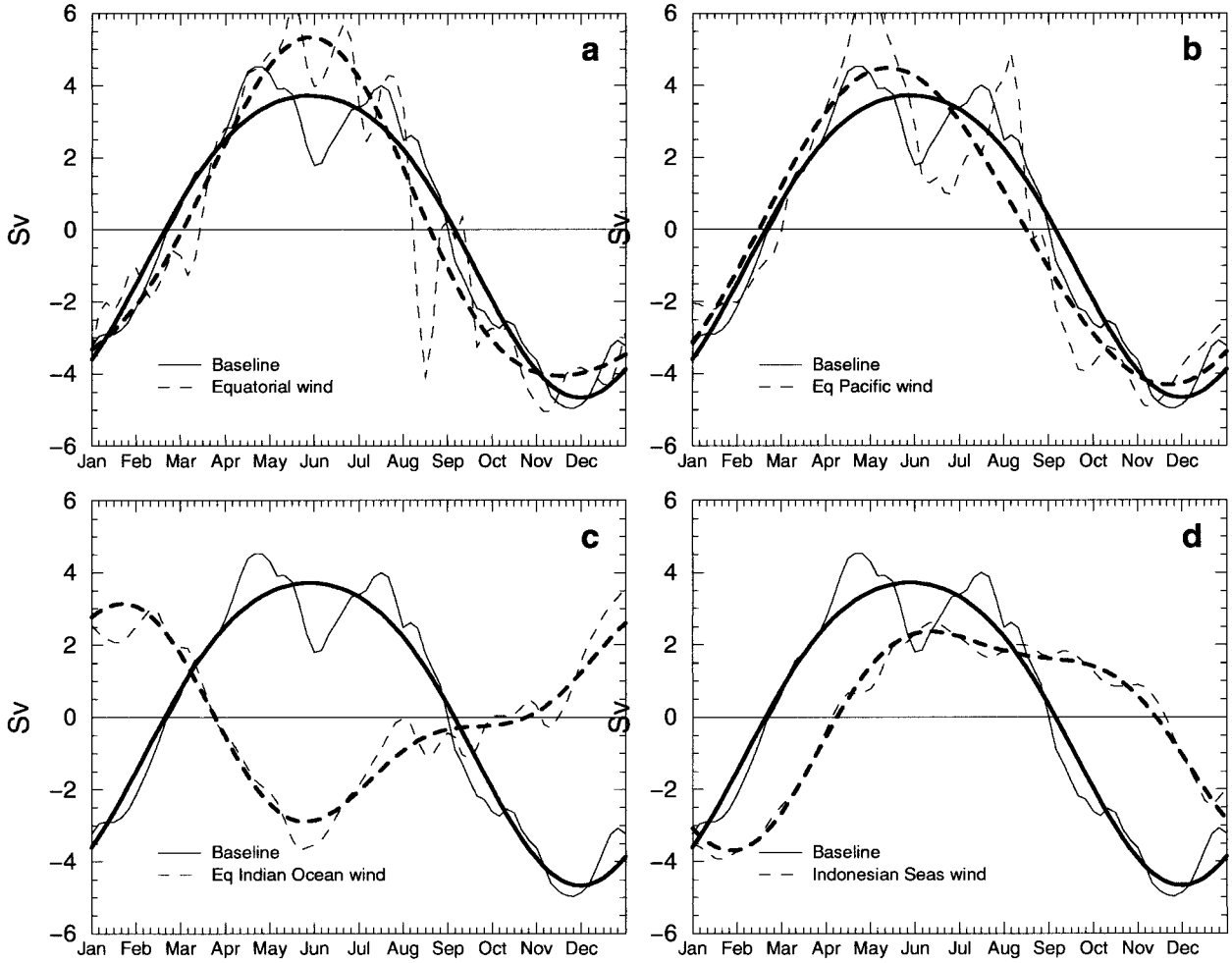

FIG. 9. Throughflow transports were computed from model experiments with time-varying wind only in certain regions. In each panel, the results from the baseline (winds varying everywhere) are shown with the solid line, results from the specific experiment are shown with the dashed line, and the annual plus semiannual harmonics are shown with the thick lines.

the upper-ocean transport was computed. For the NLOM, the top three layers represent about 400 m, while for the POCM, the top eight levels were used. Results from the current model study are also shown and are discussed in detail in section 4.

There are significant differences between the through-strait transport and the transport along the Java to Australia section for each of the models. All, however, seem to match the seasonal cycle of the observations at the Java to Australia section. The POCM has a long-term mean of 7.1 Sv through this section (in the upper eight levels, or 360 m). In April and May, it decreases to about 1 Sv, and in September it increases to 10 Sv. The peak transport is a month later than the observations and slightly less in magnitude. The NLOM transport through the Java to Australia section has a similar mean (7.7 Sv) computed from the upper three layers (about 400 m). The annual cycle is also similar to the observed estimate, except the peak in northern summer occurs earlier (in June through August).

In contrast, through-strait transport computed from the two models is less similar. The long-term mean POCM transport is very low (0.4 Sv). It has a broad peak from April through October and is very weak (about 1 Sv larger than average). The NLOM transport is much stronger (7.1 Sv) and is 4 Sv stronger in June and 4 Sv weaker in October.

A model similar to the one used in this work was applied to the Indonesian seas (Inoue and Welsh 1993). The Inoue and Welsh (1993) model is a 1½-layer, reduced-gravity model forced by climatological wind stress (Hellerman and Rosenstein 1983). A possible deficiency in this model is the placement of the open boundaries along the western (at 100°E) and southern (at 30°S) edges of the model grid, thereby eliminating remote wave effects forced outside the model domain. Nevertheless, this model produces a throughflow with a mean transport of 9.8 Sv. The variation of this transport is from a boreal winter minimum (0 Sv in February) to a broad maximum around 15 Sv from July to Sep-

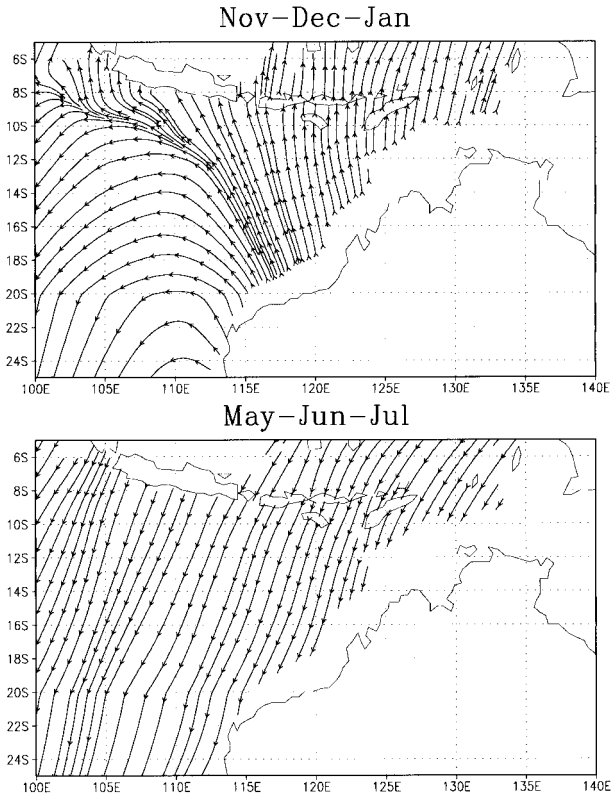

FIG. 10. Ekman velocity was computed from the Hellerman and Rosenstein (1983) wind stress data. The horizontal components are given with streamlines.

tember. The signal is mainly annual, but this may be explained by the fact that the model does not include the equatorial Indian Ocean.

The Naval Research Laboratory (NRL) also works with reduced-gravity models (e.g., NLOM), but they are much more complex in both the physics and model geometries than the Inoue and Welsh (1993) model. Kindle et al. (1987) used a 1½-layer version, spun up by climatological wind stress (Hellerman and Rosenstein 1983) and later forced by Fleet Numerical Oceanographic Center (FNOC) winds for the period from 1977 to 1984. This model has a long-term mean ITF transport of 7 Sv. The amplitude of the seasonal variations are 3.5 to 4 Sv, with the maximum transport in July/August and the minimum in January (Kindle et al. 1987). Unlike the 5½-layer version detailed in a previous section, the signal is predominantly annual.

More recently, the issue of annual variations of the throughflow transport have been investigated using coupled models. Schneider and Barnett (1997) used a coarse-resolution ocean model coupled to an atmospheric GCM to investigate the heat transport from the Pacific to the Indian Ocean via the ITF. In this model, the Pacific is connected to the Indian Ocean by two straits, but only one is used to compute ITF transport (the other, representing the Torres Strait, was too shallow for significant flow). The strait [referred to in Schneider and Barnett (1997) as the ''Indonesian Passage''] is almost 500 m deep. While their model contains a barotropic mode (unlike the present study), the depths are equivalent (about 500 m) for comparison. The Schneider and Barnett (1997) model shows no semiannual component of ITF transport, but the annual cycle has a minimum in February (7.1 Sv) and a maximum in July (20.2 Sv). Further, in this model, the barotropic component of the ITF becomes significant on longer timescales and is determined by the alongshore wind stress and winds in the southern Pacific (i.e., the island rule). The baroclinic component, however, is driven by local wind stress. Locally formed eddies also play a role. It is also pointed out that the barotropic and baroclinic signals are out of phase, although Schneider and Barnett (1997) do not see much of a semiannual signal.

3. Experiment design

To summarize the previous section, available observations and previous modeling studies do not provide a clear picture of the annual cycle of throughflow transport. It is difficult to know why there are differences between the transports from the various models without having an understanding of what is controlling the annual variations of ITF transport. The approach taken here is to intercompare the results from several experiments using one model run with various configurations.

a. Model description

The basis of this study relies on the intercomparison of several experiments to investigate the various possible forcing mechanisms for the ITF on annual timescales. Thermodynamic aspects of the ITF will not be studied, so the model used is purely hydrodynamic. Shriver and Hurlburt (1996) ran some model experiments that showed the thermohaline forcing of the throughflow accounted for almost one-third of the net transport (in their model), but acted on long timescales (longer than the annual mean). It is assumed in this study that the influence of thermohaline effects are not important to variations of the ITF mass transport on annual timescales.

Interocean exchange is obviously a focus of this study, but the large-scale ocean pathways are not addressed. For this reason, the model geometry includes the entire Indian Ocean and most of the Pacific Ocean (everything south of 35°N). There is no Atlantic Ocean in the model geometry. Further, no Antarctic Circumpolar Current (ACC) is prescribed, rather, the model grid directly connects the Pacific and Indian Oceans. The large-scale mass balance between the major ocean basins acts on a longer timescale (longer than annual), so the limit of the model in the ACC region is not an issue for this study.

The only prescribed forcing in the model is surface

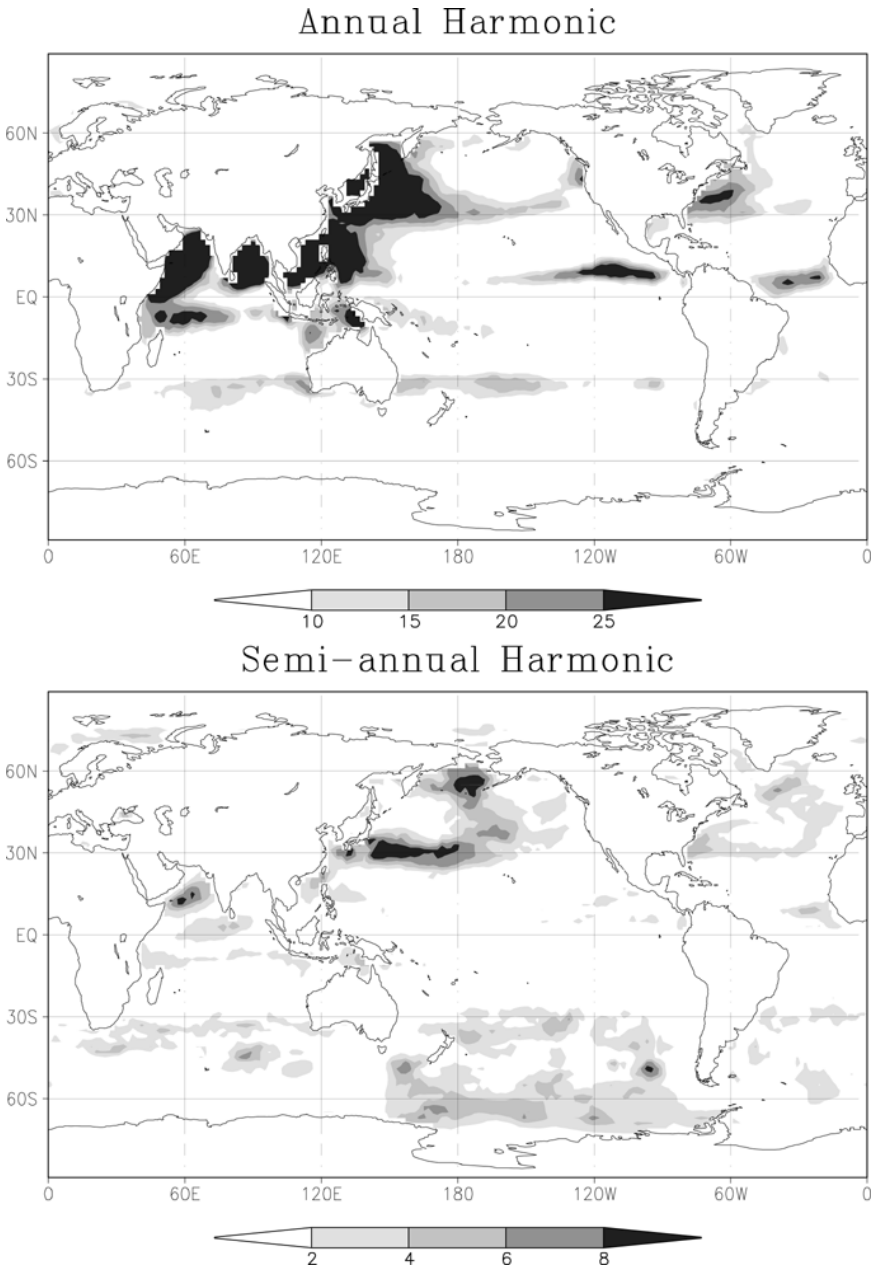

FIG. 11. The energy (power spectral density), in ($m^2\ s^{-2}$, of the annual harmonic of wind velocity computed from the Hellerman and Rosenstein (1983) wind stress dataset is given in the upper panel. The lower panel is for the semiannual harmonic. A scale is given below each panel (scale is different for each).

wind stress. For this study, climatological monthly mean winds of Hellerman and Rosenstein (1983) are used.

To further simplify the model computations and, because the throughflow appears to be mainly in the upper ocean (Fieux et al. 1994; Qu and Meyers 1995), a reduced-gravity model is used. Since the model has a quiescent lowest layer, it cannot reproduce the barotropic flow field. In addition, higher baroclinic modes are also beyond the resolution of the model (for example, only the first mode can be captured in the 1½-layer version). The second baroclinic mode can be approximated by decreasing the stratification between the two layers, however, thereby decreasing the reduced gravity. Some observations (and other model results) suggest that a substantial amount of annual variability occurs in through-strait transport at deeper levels, but the focus of this study is on upper-ocean variability, and the present model is limited to this.

The model equations are based on the hydrodynamic equations of motion. A layered, reduced-gravity for-

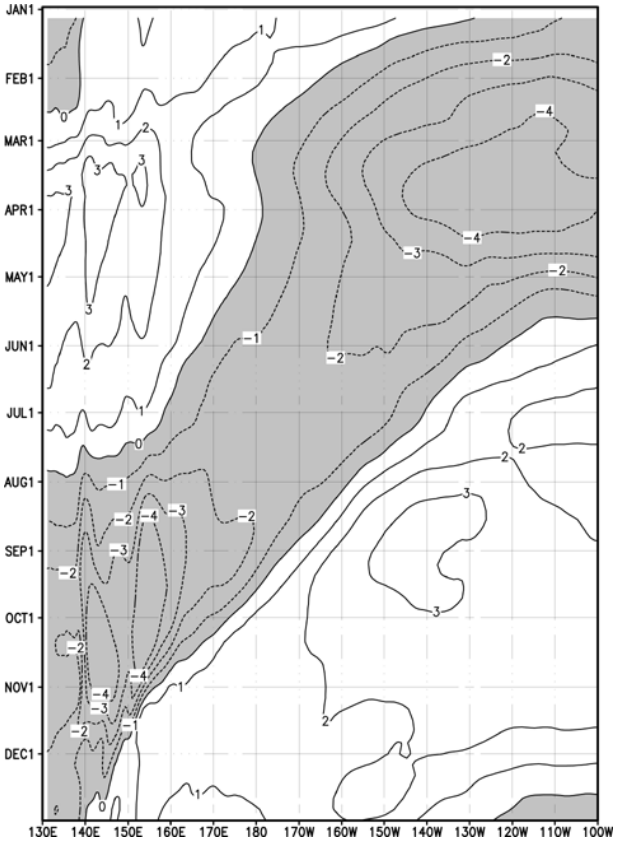

FIG. 12. Sea level anomalies along the equator in the Pacific Ocean were computed from the nonlinear model upper-layer thickness field. Negative values are shaded, and the contour interval is in centimeters.

mulation and the Boussinesq approximation are used to simplify the calculations. Layers are not permitted to have zero thickness in this formulation (no outcropping). An artificial entrainment term, w_e, has been added. Following McCreary and Kundu (1988) this value is zero unless the layer thickness goes below a specified value, h_e (set to 80 m for this study). In this case, w_e takes a finite value to maintain a minimum layer thickness. Mass is conserved by detraining an equivalent amount from the entire model domain (on timescale given by t_e, set to 1 day).

Following the ETOPO5 bathymetry (NOAA 1986), any grid points shallower than the 200-m isobath are defined as land in the model grid. The time step for all runs is 15 minutes, and output fields (u, v, h) are saved every five days. The model has a constant horizontal viscosity of 700 $m^2\ s^{-1}$. Inoue and Welsh (1993) have shown that variations in the throughflow transport are relatively independent of this value. A change of 300% (375 $m^2\ s^{-1}$ compared to 1500 $m^2\ s^{-1}$) reduced the model throughflow transport by 15% (10.5 Sv compared to 9.0 Sv), but there was no effect on the annual variability (Inoue and Welsh 1993).

b. Model experiments

The effect of the nonlinear terms was examined using three configurations of the model. In one, the full nonlinear equations were used. In another, both the momentum and continuity equations were linearized (linear equations run). To maintain stability though, the entrainment scheme (which is a nonlinear term) was needed. To understand the effect of the entrainment term, a third version was run. In this case, the forcing was reduced by 10^{-3} (reduced forcing run) to approximate a linear state (and eliminate outcropping).

The model coastlines were also varied. This is one major difference between the POCM and NLOM, and the effect is not well understood. Three model grids, shown in Fig. 4 were used. Two conform to the 200-m isobath from the $\frac{1}{12}^\circ$ ETOPO5 dataset (NOAA 1988): one with $1^\circ \times 1^\circ$ horizontal resolution everywhere, and one with higher ($\frac{1}{6}^\circ \times \frac{1}{6}^\circ$) resolution in the Indonesian region. The final experiment involving grid configuration was a model run with several islands in the Malay Archipelago treated as ocean. In this way the gap between the Pacific and the Indian Ocean was artificially widened.

Experiments were also designed to test the response of the model to surface forcing in various regions. To examine the affect of local Indonesian seas wind stress, the wind field was altered such that only the local winds (10°S–10°N, 95°–135°E) were varying in time; everywhere else in the model domain was forced by the mean December wind field. Similar experiments were run with time varying wind only in the equatorial Pacific (east of 135°E) and only in the equatorial Indian Ocean (west of 95°E; see Fig. 5). Finally, complimentary experiments were run with wind varying throughout the equatorial region (the entire band from 10°S to 10°N) and with wind varying everywhere outside the equatorial region.

4. Model results

For each configuration the model was run for 30 yr to achieve quasi-steady state (henceforth referred to as the ''baseline'' run). All wind experiments were restarted from the year 30 data and run for 5 years (experiments using different grids were run for 30 years from rest). After 3 years of model integration (initialized from the year 30 results) the amplitude and phase of the annual and semiannual harmonics of ITF transport reached equilibrium. The annual and semiannual harmonics changed by less than 2% between years 4 and 5. The results presented here are from the fifth year of integration. ITF transport was computed as the integrated transport through the three straits resolved by the model: Lombok, Ombai, and the Timor Passage (see Fig. 1 for locations). It should be noted that in this section, ITF transport refers to through-strait transport unless otherwise stated.

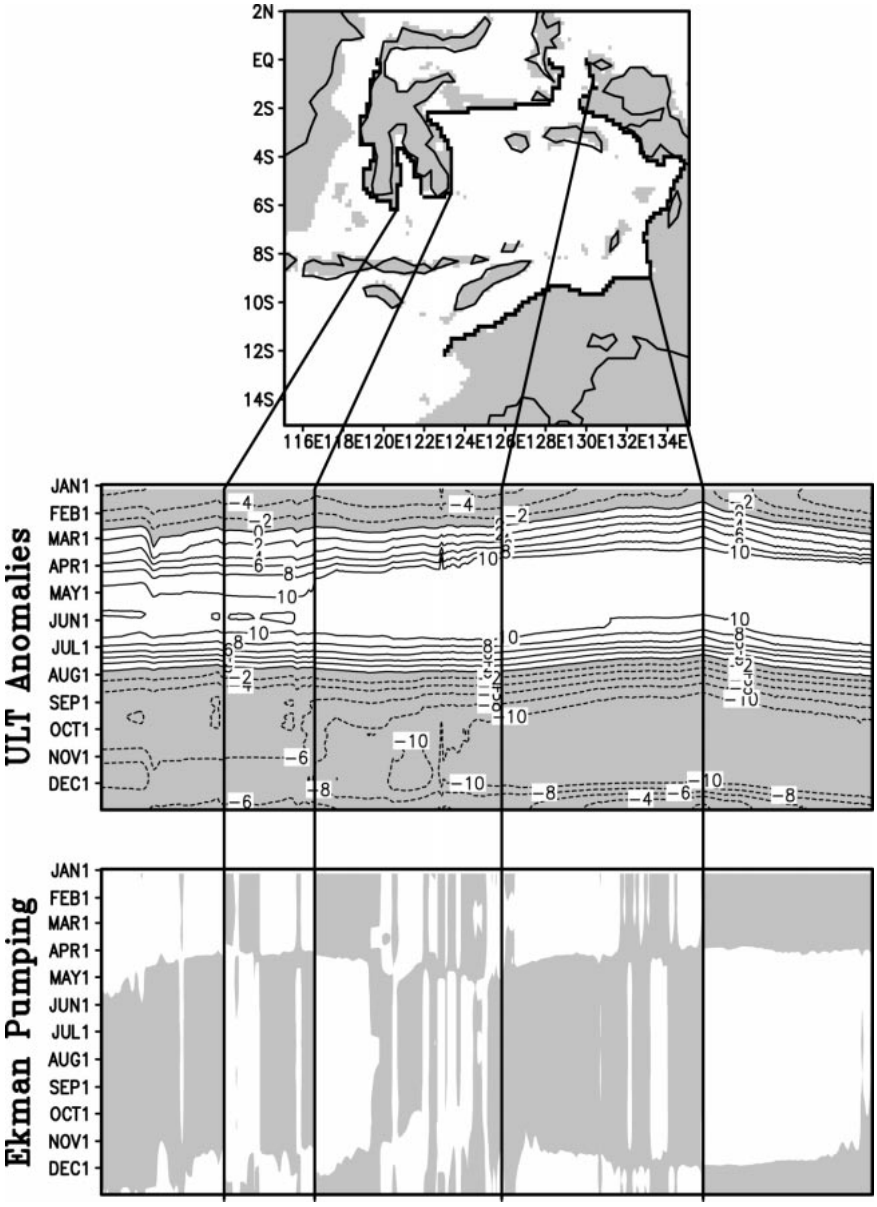

FIG. 13. Model upper-layer thickness anomalies (center panel), in meters, are given along a track (highlighted in the upper panel) that represents a coastal Kelvin wave characteristic. Ekman pumping was also computed along the same track using the Hellerman and Rosenstein (1983) wind stress data (lower panel). Shaded regions indicate upwelling. For the bottom two panels, time increases downward along the ordinate. Four black lines connect locations along the coastal path with the appropriate location in the contour plots for orientation.

The spinup of the mean through-strait transport, shown in Fig. 6, is slow (about 20 yr). This suggests that the long-term mean is a result of large-scale basin interactions. For these model experiments, it is a mass balance between the Pacific and Indian Oceans (the model does not have an Atlantic basin). In the real ocean, the long-term net transport of water through the Indonesian Throughflow is a balance between water that enters the Pacific from the Indian Ocean between Australia and Antarctica and water that exits the Pacific to the Atlantic between South America and Antarctica (neglecting secondary mass sources such as precipitation minus evaporation, river runoff, and ice melt). The ACC, therefore, plays an important role in determining the long-term mean ITF.

Unlike the long-term mean, the annual and semiannual harmonics spin up very fast (Fig. 6). For the 1½-layer nonlinear run, the phase of both the annual and semiannual harmonics change by less than a week from model year 4 to model year 30. The amplitude of the

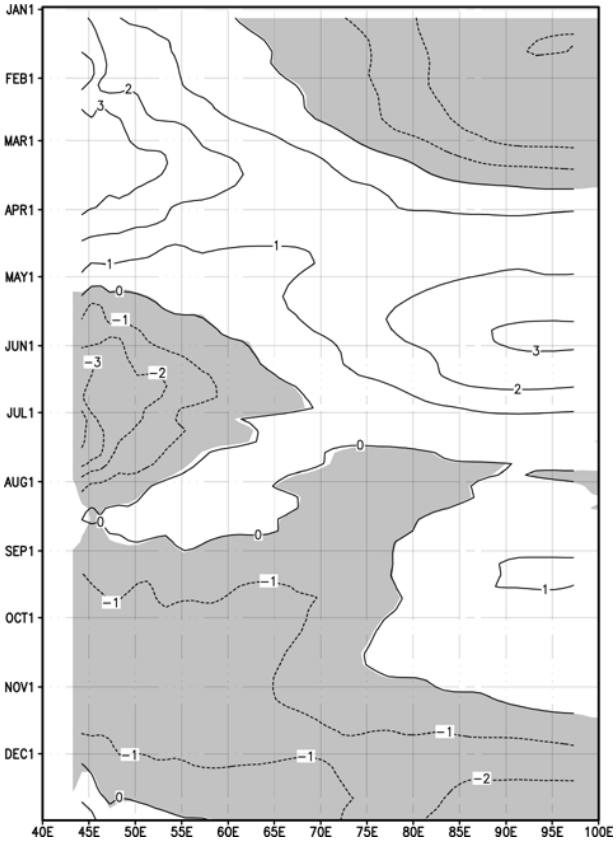

FIG. 14. Sea level anomalies along the equator in the Indian Ocean were computed from the nonlinear model upper-layer thickness field. Negative values are shaded, and the contour interval is in centimeters.

annual harmonic decreases from 4.8 Sv in year 4 to 4.2 Sv in year 30. The semiannual harmonic decreases from 1.1 to 0.5 Sv over this same period. This suggests that the annual cycle of the model throughflow is controlled either by local wind stress or remote, low-latitude wind. For remotely forced Rossby waves (east of the date line) to reach the Malay Archipelago in 4 years, they must be forced within 20° of the equator (due to the latitudinal dependence of the Rossby wave phase speed). To further examine this, the model was forced with time varying winds in certain equatorial regions.

The ITF transport from the nonlinear model run is mostly annual in period, with a peak in April through July and a minimum in November/December. The annual harmonic has a magnitude of 4.2 Sv and a semiannual harmonic of 0.5 Sv. The maximum of the annual harmonic occurs in early June.

Consistent with the hypothesis of Wyrtki (1987), throughflow transport from the model is in phase, in a gross sense, with the local wind stress. Figure 7 shows the model-derived ITF transport anomalies with a peak in northern spring/summer and a minimum in fall/winter. ITF transport is higher than average during northern spring/summer when the local winds are to the northwest. Maximum ITF transport in the model, though, occurs in June, while the peak zonal (easterly) and meridional (southerly) wind stress in the region 15°–5°S and 105°–130°E occurs in early July (see Fig. 2).

Throughflow transport was computed from the linear equations (LE) and the low forcing (LF) model runs. The ITF variability, shown in Fig. 7, is similar in all three runs. The nonlinear run has an annual harmonic with an amplitude of 4.2 Sv (maximum in early June) and a semiannual harmonic with an amplitude of 0.5 Sv (maximum in early March/September). The LF run has an annual harmonic amplitude of 3.5 Sv (maximum in early June) and a semiannual harmonic amplitude of 0.6 Sv (maximum in late June/December).

The throughflow transport computed from the NL run is very similar in amplitude and phase with the LE and LF runs. All three model runs produce ITF transports that are maximum during April through August and minimum during October through January. This similarity suggests that the variability of the throughflow on annual timescales is mainly a linear problem. This is consistent with the likelihood that Rossby/Kelvin waves are responsible for the annual cycle of transport.

To estimate the sensitivity of these results to variations of friction and coastline geometry, two additional experiments were run. In one case, the islands in the Malay Archipelago were treated as ocean points in the model (see Fig. 4). In this case, the model resolution was not changed, but the throughflow was effectively widened to 10°. The Philippine Islands, Sumatra, and Australia/New Guinea were maintained as land. The annual harmonic of the resulting throughflow was increased to 5.4 Sv (from 4.2), but the phasing did not change (see Fig. 8). The semiannual harmonic was reduced from 0.5 to 0.2 Sv.

Another model run was made with a coarser resolution. In this case, the model grid was $1° \times 1°$ everywhere (see Fig. 4). In matching the ETOPO5 bathymetry (NOAA 1986), the islands in the Indonesian seas were reduced to just four: Sulawesi, Australia/New Guinea, Halmahera, and Timor. These results are plotted in Fig. 8. Again, the annual harmonic was slightly larger (4.9 Sv). The semiannual harmonic was also larger (1.0 Sv instead of 0.5). The resulting throughflow variations still correlate well to the baseline run.

It could be anticipated that the model run with wind varying in the equatorial region would produce a throughflow similar to the baseline run, and Fig. 9 shows that this is the case. The equatorial winds did, however, produce larger annual and semiannual harmonics. In the baseline case the amplitudes are 4.2 and 0.5 Sv (annual and semiannual), while for the experiment with variable equatorial winds only, they are 4.7 and 0.7 Sv. The phasing of the semiannual component changes slightly so that the equatorial wind gives a larger throughflow than the baseline during the peak of the annual cycle (in June) and a slightly higher transport than the baseline during November, when the ITF transport is minimum.

Consistent with the idea that equatorial waves are

playing an important role, the annual cycle of ITF transport from the model run with only near-equatorial winds varying matches the transport from the LF run even better that from the NL run.

The complimentary experiment of varying winds everywhere except the near-equatorial region confirms that most forcing for the ITF on the annual timescale occurs in the near-equatorial region. In this case, the amplitude of the annual harmonic dropped to 0.6 Sv, about equal to the semiannual harmonic. The ITF transport in this case is not well correlated to the baseline run. To further examine the effect of near-equatorial winds, additional experiments were made with winds varying in three regions.

a. Local wind effects

Figure 10 shows the horizontal Ekman flow computed from the Hellerman and Rosenstein (1983) wind stress. As could be inferred from Fig. 2, the local wind pattern drives flow toward the Indian Ocean in the northern summer months. During northern winter, the Ekman flow is mainly to the north.

This is reflected in the model experiment forced by time-varying winds only in the local, Indonesian region. The results, given in Fig. 9, show a similarity to the baseline run, but the locally forced experiment has a throughflow with an annual harmonic peak in late July (compared to the baseline run with a peak annual harmonic in early June). In addition, the locally forced experiment annual harmonic amplitude (2.8 Sv) is three times the semiannual (0.9 Sv). With only local varying winds, the ITF has a broad maximum from June through October.

b. Remote wind effects

The case forced by winds varying only in the equatorial Indian Ocean, shown in Fig. 9, gives the most dramatic change to the ITF. In this experiment, the ITF has a maximum in late January and a minimum in late May. The annual harmonic amplitude is 2.4 Sv and the amplitude of the semiannual harmonic is 1.1 Sv. Clarke and Liu (1993) speculated that semiannual signals in the throughflow were driven by variations on the Indian Ocean side of the ITF region, specifically the semiannual Kelvin waves generated during the monsoon transition. (Masumoto and Yamagata 1996) later examined this in a modeling study and found that Lombok Strait (the westernmost strait) had the highest semiannual component. The observations, at least for the two individual years studied, show no semiannual signal in Lombok transport (Murray and Arief 1988), but a relatively strong one in the lower layer of the Timor Passage (Molcard et al. 1996). In the experiment with winds varying only in the equatorial Indian Ocean, flow in all three straits (Lombok, Ombai, and Timor) have annual harmonics twice the amplitude of the semiannual. The model run with only Indian Ocean winds does, however, produce a larger semiannual to annual harmonic ratio (it is 0.1 for the baseline run and 0.5 for the Indian Ocean wind experiment).

ITF transport from the model forced by winds varying in the entire equatorial Pacific is very similar to the baseline run (see Fig. 9). The annual harmonic is larger in the equatorial Pacific wind case than the baseline run (4.4 Sv compared to 4.2 Sv) and the phase is slightly smaller (the ITF peaks 12 days earlier in the equatorial Pacific wind experiment). The semiannual harmonic is only 0.1 Sv when only equatorial Pacific winds are varied in time.

In summary, the seasonal variability in through-strait transport in the wind-forced model is due to winds in the equatorial region (10°N to 10°S). Local winds appear to counter the effects of remote, equatorial Indian Ocean winds, and the model run with varying winds only in the equatorial Pacific has ITF variability similar to the baseline run.

5. Discussion

a. Equatorial forcing mechanisms

Equatorial Rossby waves are one possible mechanism for how equatorial Pacific winds can be responsible for the seasonal cycle of the ITF. Figure 11 shows the energy in the annual and semiannual harmonics of the wind field. A large annual signal is seen just north of the equator in the eastern Pacific. In the model, the resulting Ekman suction generates an upwelling Rossby wave in late winter/spring that propagates west across the basin to the western boundary of the Pacific by fall. In summer, Ekman pumping forces a downwelling wave. The phase of these Rossby waves is in agreement with observations (Meyers 1979; Lukas and Firing 1985; Kessler 1990). The arrival of these upwelling and downwelling waves, seen in Fig. 12, is coincident with the minimum and maximum in throughflow transport. In the model, these Rossby waves interact with the western boundary of the Pacific and create coastal Kelvin waves. Figure 13 shows the propagation of the coastal waves through the Indonesian seas. In this figure, the local Ekman pumping is also shown. Due to changes in coastline configuration, the vertical Ekman velocity changes sign abruptly, but the model sea level anomalies along the coast are continuous (the integrated effect of Ekman pumping on the coastal wave along its characteristic is neither constructive nor destructive).

On the Indian Ocean side of the throughflow, Kelvin waves also play a role in adjusting sea level. During certain times of the year, however, the alongshore Ekman pumping acts to dampen the coastal waves. Figure 14 shows the model sea level along the equator in the Indian Ocean. Westerly winds during the monsoon transitions create convergence at the equator, and downwelling (positive sea level anom-

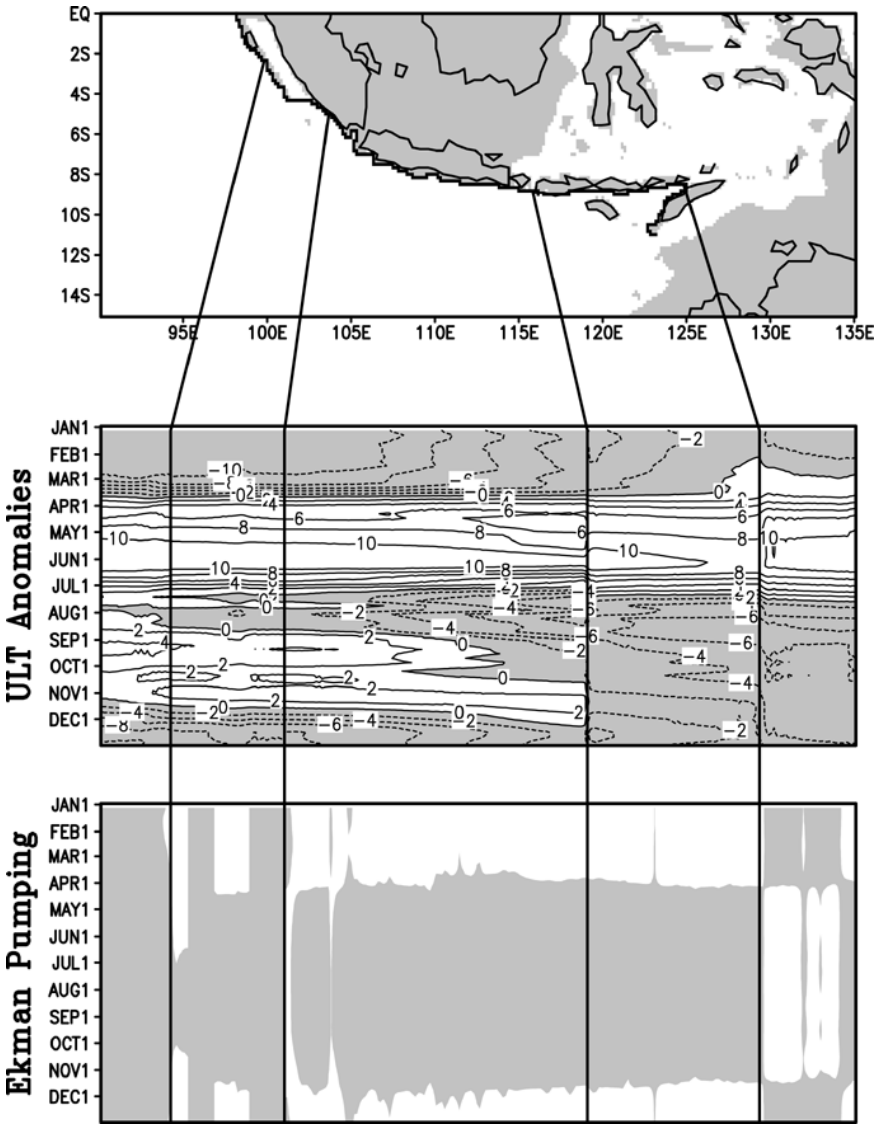

FIG. 15. Model upper-layer thickness anomalies (center panel), in meters, are given along a track (highlighted in the upper panel) that represents a coastal Kelvin wave characteristic. Ekman pumping was also computed along the same track using the Hellerman and Rosenstein (1983) wind stress data (lower panel). Shaded regions indicate upwelling. For the bottom two panels, time increases downward along the ordinate. Four black lines connect locations along the coastal path with the appropriate location in the contour plots for orientation.

aly) Kelvin waves are formed (Wyrtki 1973; O'Brien and Hurlburt 1974). These waves take about 40–50 days to reach the eastern boundary of the Indian Ocean. The model has peak positive sea level anomalies on the eastern boundary of the equatorial Indian Ocean in early June and mid-September. The mid-September peak is somewhat weaker than in June (1 cm compared to 3 cm). In northern winter, during the northeast monsoon, an upwelling Kelvin wave is formed, bringing negative sea level anomalies to the west coast of Sumatra.

In the model, these Kelvin waves affect the ITF by modifying sea level along the southern coasts of Sumatra and Java. Equatorial Kelvin waves form two coastal Kelvin waves when they reach the eastern boundary of the Indian Ocean. The one propagating southward reaches the Indonesian straits in just a few days. The effects of these waves are evident in both observations (Quadfasel and Cresswell 1992) and the model experiments of this study.

Unlike the Pacific side of the throughflow, local wind stress along the Indian Ocean side of the ITF acts to dampen the Kelvin-wave-produced sea level anomalies. Figure 15 shows the vertical Ekman velocity is negative (upwelling) during April through November for most of the southern coastline of the Sunda Islands. This

upwelling acts to dampen the downwelling Kelvin wave in northern fall, and the resulting sea level east of the Lombok Strait is mostly annual. The result therefore, in the model, is that sea level on the Indian Ocean side of the ITF is high in March through July and low during the rest of the year.

The relatively short time required to spin up the model ITF annual and semiannual harmonics (four years) indicates the controlling mechanism is either local or near equatorial. The similarity of the nonlinear and linear runs is consistent with the idea that equatorial waves dominate. The change in grid spacing without a change in ITF variability also supports this idea.

Finally, it should be noted that a fundamental result of this work is that ITF transport variability (measured across outflow straits in the upper ocean) is determined by a combination of equatorial Pacific winds, equatorial Indian Ocean winds, and local (Indonesian) winds. For the particular case of this study, the local winds in the Indonesian region cancel the effects from the equatorial Indian Ocean, thus leaving the remote Pacific winds to dominate the signal. Wind data, in general, is poor in the equatorial Indian Ocean, and other wind products would probably not produce signals that directly cancel. The exact phasing and amplitude of the winds in each region remains to be determined.

b. Model comparison

The present study was partially motivated by trying to understand why different models give different ITF variability on the annual timescale, and the results show the importance of equatorial winds. In section 2c, the annual cycle of through-strait transport computed from the output of two OGCM's was discussed (results shown in Fig. 3). To compare directly to observations, the transport was computed above approximately 400 m along a track from Java to Australia (long-term mean removed). Transport variations from the three models match the observations fairly well along this track. The UHLM has a slightly smaller amplitude and is missing the fall minimum. This could be due to the weak fall Kelvin wave in the UHLM (which would elevate sea level on the Indian Ocean side and reduce the throughflow).

While the three models have fairly good agreement in upper-ocean transport along this section, the through-strait transport computed from these models (also shown in Fig. 3) shows more of a difference, suggesting that there is a different forcing mechanism for transport at the two locations. The results presented in the previous section can be used to explain the differences in the through-strait transport variations. The POCM has a very weak annual amplitude, about 1 Sv, and it has a broad peak from April through October. This is consistent with the local wind forcing, which is to the northwest during this time. The POCM was forced by ECMWF wind stress, and the annual Rossby waves generated have a smaller amplitude (free surface variations from the POCM range from ± 5 cm along 5°N). The NLOM shows more annual variation, from $+4$ Sv in April to -4 Sv in October. The results from this model agree very well with the model used in this study (UHLM), with perhaps a month lag between the two. This is consistent with the hypothesis presented, since despite having different physics, the two model were seasonally forced by Hellerman and Rosenstein (1983) wind stress (the NLOM, though, adds ECMWF anomalies to the mean seasonal cycle).

In conclusion, these results, while providing an explanation for seasonal variability of the throughflow, also highlight two outstanding issues. First, there seems to be a significant difference in through-strait transport and transport along the Meyers et al. (1995) transect. This is true for the models (Fig. 3) and the observations (see Fig. 1). Second, there is a difference between the baroclinic transport and barotropic transport in the throughflow region. While this study only can address the baroclinic component, other model studies (e.g., Schneider and Barnett 1997; Schiller et al. 1998) have investigated the barotropic component. Further study of these two issues is the focus of ongoing work.

Acknowledgments. This work is the result of the assistance of numerous people. The author is especially grateful to Roger Lukas who provided constant intellectual guidance and financial support. Numerous discussions with Bo Qiu were also invaluable. Stuart Godfrey provided a careful, in-depth review that greatly improved the manuscript. The author is also indebted to Kathy Donohue, Dail Rowe, and Niklas Schneider for stimulating discussions. Finally, the comments of an anonymous reviewer are gratefully acknowledged. Financial support of this work was provided by JAMSTEC Grant 434957, JPL 958120, NAS5-31722, NSF OCE 9024452, NSF OCE 9113948, NSF OCE 9216891, and NSF OCE 9525986.

REFERENCES

Clarke, A. J., and X. Liu, 1993: Observations and dynamics of semiannual and annual sea levels near the eastern equatorial Indian Ocean boundary. *J. Phys. Oceanogr.,* **23,** 386–399.

——, and ——, 1994: Interannual sea level in the northern and eastern Indian Ocean. *J. Phys. Oceanogr.,* **24,** 1224–1235.

Fieux, M., C. Andrie, P. Delecluse, A. G. Ilahude, A. Kartavseff, F. Mantisi, R. Molcard, and J. C. Swallow, 1994: Measurements within the Pacific–Indian Oceans throughflow region. *Deep-Sea Res.,* **41,** 1091–1130.

Godfrey, J. S., 1989: A Sverdrup model of the depth-integrated flow for the world ocean allowing for island circulations. *Geophys. Astrophys. Fluid Dyn.,* **45,** 89–112.

——, 1996: The effect of the Indonesian throughflow on ocean circulation and heat exchange with the atmosphere: A review. *J. Geophys. Res.,* **101,** 12 217–12 238.

Hellerman, S., and M. Rosenstein, 1983: Normal monthly wind stress over the world ocean with error estimates. *J. Phys. Oceanogr.,* **13,** 1093–1104.

Inoue, M., and S. E. Welsh, 1993: Modeling seasonal variability in

the wind-driven upper-layer circulation in the Indo–Pacific region. *J. Phys. Oceanogr.,* **23,** 1411–1436.
Kessler, W. S., 1990: Observations of long Rossby waves in the northern tropical Pacific. *J. Geophys. Res.,* **95,** 5183–5217.
Kindle, J., G. W. Heburn, and R. C. Rhodes, 1987: An estimate of the Pacific to Indian Ocean througflow from a global numerical model. Further Progress in Equatorial Oceanography, E. J. Katz and J. M. Whitte, Eds., Nova University Press, 317–321.
Lukas, R., and E. Firing, 1985: The annual Rossby wave in the central equatorial Pacific Ocean. *J. Phys. Oceanogr.,* **15,** 55–67.
——, ——, P. Hacker, P. L. Richardson, C. A. Collins, R. Fine, and R. Gammon 1991: Observations of the Mindanao Current during the Western Equatorial Pacific Ocean Circulation Study. *J. Geophys. Res.,* **96,** 7089–7104.
——, T. Yamagata, and J. P. McCreary, 1996: Pacific Ocean low latitude western boundary currents and the Indonesian throughflow. *J. Geophys. Res.,* **101,** 12 209–12 216.
Masumoto, Y., and T. Yamagata, 1996: Seasonal variations of the Indonesian throughflow in a general ocean circulation model. *J. Geophys. Res.,* **101,** 12 287–12 293.
McCreary, J., and P. Kundu, 1988: Thermohaline forcing of eastern boundary currents with application to the circulation off the west coast of Australia. *J. Mar. Res.,* **46,** 25–58.
Meyers, G., 1979: On the annual Rossby wave in the tropical north Pacific. *J. Phys. Oceanogr.,* **9,** 663–674.
——, 1996: Variation of Indonesian throughflow and ENSO. *J. Geophys. Res.,* **101,** 12 255–12 264.
——, R. J. Bailey, and A. P. Worby, 1995: Volume transport of Indonesian through-flow. *Deep-Sea Res.,* **42,** 1163–1174.
Molcard, R., M. Fieux, and A. G. Ilahude, 1996: The Indo–Pacific throughflow in the Timor Passage. *J. Geophys. Res.,* **101,** 12 411–12 420.
Murray, S. P., and D. Arief, 1988: Throughflow into the Indian Ocean through the Lombok Strait, January 1985–January 1986. *Nature,* **333,** 444–447.
Nicholls, N., 1984: The Southern Oscillation and Indonesian sea surface temperature. *Mon. Wea. Rev.,* **112,** 424–432.
NOAA, 1988: Data Announcement 88-MGG-02, Digital relief of the surface of the earth. NOAA, National Geophysical Data Center, Boulder, CO.
Nof, D., 1995: Choked flows from the Pacific to the Indian Ocean. *J. Phys. Oceanogr.,* **25,** 1369–1383.
O'Brien, J. J., and H. E. Hurlburt, 1974: Equatorial jet in the Indian Ocean: Theory. *Science,* **184,** 1075–1077.
Pedlosky, J., L. J. Pratt, M. A. Spall, and K. R. Helfrich, 1999: Circulation around islands and ridges. *J. Mar. Res.,* **55,** 1199–1251.
Pratt, L., and J. Pedlosky, 1998: Barotropic circulation around islands with friction. *J. Phys. Oceanogr.,* **28,** 2148–2162.
Qiu, B., M. Mao, and Y. Kashino, 1999: Intraseasonal variability in the Indo–Pacific throughflow and the regions surrounding the Indonesian seas. *J. Phys. Oceanogr.,* **29,** 1599–1618.
Qu, T., and G. Meyers, 1995: A method to estimate dynamic height and geostrophic transport relative to deeper levels from 400m expendable bathythermograph in the Indonesian throughflow. *Chin. J. Oceanol. Limnol.,* **13,** 97–109.
——, ——, J. S. Godfrey, and D. Hu, 1994: Ocean dynamics in the region between Australia and Indonesia and its influence on the variation of sea surface temperature in a global general circulation model. *J. Geophys. Res.,* **99,** 18 433–18 445.
Quadfasel, D., and G. R. Cresswell, 1992: A note on the seasonal variability of the South Java Current. *J. Geophys. Res.,* **97,** 3685–3688.
Schiller, A., J. S. Godfrey, P. C. McIntosh, G. Meyers, and S. E. Wijffels, 1998: Seasonal near-surface dynamics and thermodynamics of the Indian Ocean and Indonesian throughflow in a global ocean general circulation model. *J. Phys. Oceanogr.,* **28,** 2288–2312.
Schneider, N., and T. P. Barnett, 1997: Indonesian throughflow in a coupled general circulation model. *J. Geophys. Res.,* **102,** 12 314–12 358.
Semtner, A. J., and R. M. Chervin, 1988: A simulation of the global ocean circulation with resolved eddies. *J. Geophys. Res.,* **93,** 15 502–15 522.
Shriver, J. F., and H. E. Hurlbutt, 1996: The contribution of the global thermohaline circulation to the Pacific to Indian Ocean throughflow via Indonesia. *J. Geophys. Res.,* **102,** 5491–5512.
Trenberth, K. E., W. G. Large, and J. G. Olson, 1990: The mean annual cycle in global ocean wind stress. *J. Phys. Oceanogr.,* **20,** 1742–1760.
Wajsowicz, R. C., 1993: The circulation of the depth-integrated flow around an island with application to the Indonesian throughflow. *J. Phys. Oceanogr.,* **23,** 1470–1484.
——, 1995: The response of the Indo-Pacific throughflow to interannual variations in the Pacific wind stress. Part I. *J. Phys. Oceanogr.,* **25,** 1805–1826.
Wallcraft, A. J., 1991: The Navy Layered Ocean Model user's guide. Rep. 35, NOARL, 21 pp.
Wyrtki, K., 1961: Physical oceanography of the southeast Asian waters. NAGA Rep 2, Scripps Institute of Oceanography, 195 pp.
——, 1973: An equatorial jet in the Indian Ocean. *Science,* **181,** 262–264.
——, 1987: Indonesian throughflow and the associated pressure gradient. *J. Geophys. Res.,* **92,** 12 941–12 946.